

ICES REPORT 12-07

January 2012

Isogeometric collocation for elastostatics and explicit dynamics

by

F. Auricchio, L. Beirao da Veiga, T.J.R. Hughes, A. Reali, G. Sangalli



The Institute for Computational Engineering and Sciences
The University of Texas at Austin
Austin, Texas 78712

Reference: F. Auricchio, L. Beirao da Veiga, T.J.R. Hughes, A. Reali, G. Sangalli, Isogeometric collocation for elastostatics and explicit dynamics, ICES REPORT 12-07, The Institute for Computational Engineering and Sciences, The University of Texas at Austin, January 2012.

Report Documentation Page

Form Approved
OMB No. 0704-0188

Public reporting burden for the collection of information is estimated to average 1 hour per response, including the time for reviewing instructions, searching existing data sources, gathering and maintaining the data needed, and completing and reviewing the collection of information. Send comments regarding this burden estimate or any other aspect of this collection of information, including suggestions for reducing this burden, to Washington Headquarters Services, Directorate for Information Operations and Reports, 1215 Jefferson Davis Highway, Suite 1204, Arlington VA 22202-4302. Respondents should be aware that notwithstanding any other provision of law, no person shall be subject to a penalty for failing to comply with a collection of information if it does not display a currently valid OMB control number.

1. REPORT DATE 30 JAN 2012		2. REPORT TYPE		3. DATES COVERED 00-00-2012 to 00-00-2012	
4. TITLE AND SUBTITLE Isogeometric collocation for elastostatics and explicit dynamics				5a. CONTRACT NUMBER	
				5b. GRANT NUMBER	
				5c. PROGRAM ELEMENT NUMBER	
6. AUTHOR(S)				5d. PROJECT NUMBER	
				5e. TASK NUMBER	
				5f. WORK UNIT NUMBER	
7. PERFORMING ORGANIZATION NAME(S) AND ADDRESS(ES) University of Texas at Austin, Institute for Computational Engineering and Sciences, Austin, TX, 78712				8. PERFORMING ORGANIZATION REPORT NUMBER	
9. SPONSORING/MONITORING AGENCY NAME(S) AND ADDRESS(ES)				10. SPONSOR/MONITOR'S ACRONYM(S)	
				11. SPONSOR/MONITOR'S REPORT NUMBER(S)	
12. DISTRIBUTION/AVAILABILITY STATEMENT Approved for public release; distribution unlimited					
13. SUPPLEMENTARY NOTES					
14. ABSTRACT We extend the development of collocation methods within the framework of Isogeometric Analysis (IGA) to multi-patch NURBS configurations, various boundary and patch interface conditions, and explicit dynamic analysis. The methods developed are higher-order accurate, stable with no hourglass modes, and efficient in that they require a minimum number of quadrature evaluations. The combination of these attributes has not been obtained previously within standard finite element analysis.					
15. SUBJECT TERMS					
16. SECURITY CLASSIFICATION OF:			17. LIMITATION OF ABSTRACT Same as Report (SAR)	18. NUMBER OF PAGES 36	19a. NAME OF RESPONSIBLE PERSON
a. REPORT unclassified	b. ABSTRACT unclassified	c. THIS PAGE unclassified			

Isogeometric collocation for elastostatics and explicit dynamics

F. Auricchio^{a,c}, L. Beirão da Veiga^{b,c}, T.J.R. Hughes^d,
A. Reali^{a,c,*}, G. Sangalli^{e,c}

^a*Structural Mechanics Department, University of Pavia*

^b*Mathematics Department “F. Enriques”, University of Milan*

^c*IMATI-CNR, Pavia*

^d*Institute for Computational Engineering and Sciences, University of Texas at Austin*

^e*Mathematics Department, University of Pavia*

Abstract

We extend the development of collocation methods within the framework of Isogeometric Analysis (IGA) to multi-patch NURBS configurations, various boundary and patch interface conditions, and explicit dynamic analysis. The methods developed are higher-order accurate, stable with no hourglass modes, and efficient in that they require a minimum number of quadrature evaluations. The combination of these attributes has not been obtained previously within standard finite element analysis.

Key words: Isogeometric analysis; collocation methods; B-splines; NURBS; explicit dynamics.

1 Introduction

There are many application areas of finite element analysis in which the efficiency and success of the methodology is directly related to the number of

* Corresponding author.

Address: Structural Mechanics Department, University of Pavia

Via Ferrata 1, 27100, Pavia, Italy.

Phone: +39-0382-98704. Fax: +39-0382-528422

E-mail: alessandro.reali@unipv.it

quadrature points needed to integrate arrays. The most salient example is explicit dynamic analysis in which the predominant cost is determined by the residual force calculation and, in particular, the evaluation of stresses at quadrature points. In this case, storage and compute cost are directly proportional to the number of quadrature points. Typical commercial explicit codes, which represent the dominant technologies utilized in crash analysis and metal forming, typically employ low-order elements, usually four-node quadrilateral shell elements with one through-thickness stack of quadrature points, and eight-node hexahedral elements in three-dimensional solid analysis with one quadrature point. The location of the quadrature points is at the origin of parametric coordinates within the element, that is, the one-point Gauss rule. This minimizes storage of stresses and the number of constitutive evaluations and results in an efficient computational procedure for very large industrial problems. However, there are shortcomings engendered by one-point quadrature for which no completely satisfactory solutions have been found.

The most prominent shortcoming is that one-point quadrature results in rank deficiency of the discrete system. The poster child for this phenomenon is the famous “hourglass mode”, although other modes of deformation also give rise to singularities (see, e.g., Chapters 4.6 and 5.3 in [25]). For simplicity of vocabulary, henceforth we will simply refer to all spurious singular modes as hourglass modes.

There has been a very large number of papers devoted to stabilizing hourglass modes by artificial viscous and elastic mechanisms, but the commonly used techniques are ad hoc and involve parameters that require tuning. If the parameters are too small, mesh instabilities appear, if they are too large, physical response is altered. In many cases the happy medium is difficult to predict. If runs need to be repeated and parameters adjusted in trial and error fashion, engineering and computer time are wasted.

Another shortcoming is the low-order accuracy of standard explicit dynamics algorithms. The hope of achieving higher-order accuracy in explicit finite element technology seems to have been lost long ago. Why has this occurred? In our view it has to do with the discrete spectrum of higher-order finite elements. As the degree of polynomials is increased, the lower modes become more accurate, which is theoretically well understood, but the higher modes diverge with polynomial degree, a surprising result that was discovered recently in the investigations of [15,28,36]; see also [14]. These many “bad” modes are not much of an issue in elliptic (e.g., static elastic) or parabolic (e.g., heat conduction) problems, due to the strong stability of these operators, but they are a significant problem in hyperbolic (e.g., structural dynamic) problems and, in particular, ones in which high modal behavior is unavoidable, such as during impact in crash dynamics. Higher-order finite elements exhibit a lack of robustness in these cases. Low-order finite elements have the advantage that

their higher modes are better behaved than those of high-order finite elements, and this seems to be an important reason for the preference of low-order elements. Poor practical experiences, which years ago led to the elimination of higher-order elements in explicit codes, such as LS DYNA, may also be attributed to these negative results for higher-order finite elements. However, based on recent innovations, we believe that there may be alternatives to what currently exists.

One direction that may be pursued in an effort to develop better minimal-quadrature-point discretization technology is collocation, but within the framework of Isogeometric Analysis (IGA), which has been the subject of numerous recent studies [1–16,19,21,22,24,26,28,29,36,39,40] , rather than within traditional finite element analysis. IGA utilizes smooth basis functions emanating from computer aided geometric design, for example, NURBS, T-splines, etc. The *raison d'être* of IGA is to simplify the generation of finite element models from CAD designs by utilizing a single mathematical representation for both design and analysis. However, IGA has also been shown to be a superior computational mechanics technology to traditional finite elements in many situations [ibid.]. In particular, and of importance in hyperbolic cases, is that, unlike traditional finite elements, the higher modes of IGA basis functions do not diverge with increasing degree, but in fact achieve almost spectral accuracy that improves with degree. It has been shown that the robustness of higher-order NURBS elements increases with polynomial degree [32], in contrast with the behavior of higher-order finite elements. This deficiency of traditional higher-order finite elements is overcome by IGA.

The smoothness of IGA basis functions enables use of the strong form of the partial differential equations, which provides a platform for collocation with interesting stability properties. Collocation may be viewed as a variant of one-point quadrature. It is simple to show that for quadratic and higher-order NURBS, with uniform knot vectors and a suitable choice of the collocation points, the discrete Laplace operator produced by collocation is rank sufficient in all dimensions. It follows that the elasticity operator is also rank sufficient, that is, no hourglass modes. This is in contrast with one-point quadrature on low-order finite elements, as described above. The upshot of this observation is that IGA collocation methods eliminate the need for ad hoc hourglass stabilization techniques and their tuning parameters.

Based on the previous discussion, IGA collocation opens the way to stable, robust, higher-order accurate methods with a minimum number of quadrature points. In order to take advantage of these attributes in explicit dynamics, one must use lumped mass matrices. A unique, positive, lumped mass matrix may be computed for IGA by the row-sum technique (see [25], Chapter 7.3). Unfortunately, the lumped mass matrix does not maintain the accuracy of the consistent mass matrix. This has been noted in our previous studies [15,28,14].

In fact, accuracy is limited to second-order no matter the polynomial degree, and accuracy degrades very significantly in higher modes (see also [39]). A solution to this dilemma is provided by the explicit predictor multi-corrector algorithms described in (see [27], Chapter 9.4 in [25] and Chapter 6.2.3 in [14]) in which the lumped mass is used as the diagonal “left-hand-side” matrix and the consistent mass is used in the “right-hand-side” residual vector calculation. This preserves the usual explicit computational architecture and through corrector iterations is able to maintain the spatial accuracy of consistent mass.

The combination of the technologies described above provides the potential for efficient, stable, robust and higher-order accurate explicit dynamics methods. This paper is devoted to pursuing the issues arising in the development of this methodology. It builds on our earlier work [3] in which we introduced a collocation scheme for a single NURBS patch. In [3] we provided a complete mathematical analysis of the one-dimensional case. The results of the mathematical analysis are not applicable in multiple dimensions and thus this remains an open problem. However, we confirmed the theoretical convergence rates numerically on linear elliptic problems in one, two and three dimensions. We also numerically investigated the discrete eigenspectrum and the effects of alternative locations of collocation points.

An outline of this paper follows:

In Section 2 we briefly review some basic results on B-splines, NURBS and the resulting element structure of multi-patch configurations.

In Section 3 we start with a standard variational formulation for the linear elastostatic problem and, invoking sufficient smoothness of the function spaces, integrate by parts to yield the strong form of the residual within patches and traction continuity conditions on patch interfaces and external boundaries. We do not assume the test function space is the same as the solution space. We then use standard techniques to construct C^∞ test functions with compact support that comprise Dirac delta sequences about each of the desired collocation points. Taking the limit of the sequences, defines the collocation scheme. Special consideration needs to be given to points on the patch interfaces and external boundaries and we give precise descriptions of the treatment of several important cases.

In Section 4 we generalize to dynamics and describe the explicit predictor multi-corrector time integration algorithms. We argue that if a sufficient number of explicit multi-corrector iterations is utilized, the higher-order spatial accuracy of the corresponding implicit algorithm with consistent mass is achieved.

In Section 5 we present several static numerical examples. We test the method on Dirichlet and Neumann boundary conditions, mixed boundary conditions, and on single and multi-patch configurations with different material properties

in the patches. Satisfactory results are obtained in all cases.

In Section 6 we present dynamic cases. We confirm the higher-order convergence rates of the explicit multi-corrector method on a one-dimensional example and a two dimensional plane strain annular configuration.

We draw conclusions in Section 7.

2 NURBS-based isogeometric analysis

Non-Uniform Rational B-splines (NURBS) are a standard tool for describing and modeling curves and surfaces in computer aided design and computer graphics (see Piegl and Tiller [34] and Rogers [37] for an extensive description of these functions and their properties). In this work, we use NURBS as an analysis tool, as proposed by Hughes *et al.* [26]. The aim of this section is to present a short description of B-splines and NURBS, followed by a simple discussion on the basics of isogeometric analysis and by an introduction to the proposed collocation method.

2.1 B-splines and NURBS

B-splines in the plane are piecewise polynomial curves composed of linear combinations of B-spline basis functions. The coefficients (\mathbf{B}_i) are points in the plane, referred to as *control points*.

A *knot vector* is a set of non-decreasing real numbers representing coordinates in the parametric space of the curve

$$\{\xi_1 = 0, \dots, \xi_{n+p+1} = 1\}, \quad (1)$$

where p is the order of the B-spline and n is the number of basis functions (and control points) necessary to describe it. The interval $[\xi_1, \xi_{n+p+1}]$ is called a *patch*. A knot vector is said to be *uniform* if its knots are uniformly-spaced and *non-uniform* otherwise; it is said to be *open* if its first and last knots have multiplicity $p + 1$. In what follows, we always employ open knot vectors. Basis functions formed from open knot vectors are interpolatory at the ends of the parametric interval $[0, 1]$ but are not, in general, interpolatory at interior knots.

Given a knot vector, univariate B-spline basis functions are defined recursively

starting with $p = 0$ (piecewise constants)

$$N_{i,0}(\xi) = \begin{cases} 1 & \text{if } \xi_i \leq \xi < \xi_{i+1} \\ 0 & \text{otherwise.} \end{cases} \quad (2)$$

For $p > 1$:

$$N_{i,p}(\xi) = \begin{cases} \frac{\xi - \xi_i}{\xi_{i+p} - \xi_i} N_{i,p-1}(\xi) + \frac{\xi_{i+p+1} - \xi}{\xi_{i+p+1} - \xi_{i+1}} N_{i+1,p-1}(\xi) & \text{if } \xi_i \leq \xi < \xi_{i+p+1} \\ 0 & \text{otherwise,} \end{cases} \quad (3)$$

where, in (3), we adopt the convention $0/0 = 0$.

In Figure 1 we present an example consisting of $n = 9$ cubic basis functions generated from the open knot vector $\{0, 0, 0, 0, 1/6, 1/3, 1/2, 2/3, 5/6, 1, 1, 1, 1\}$.

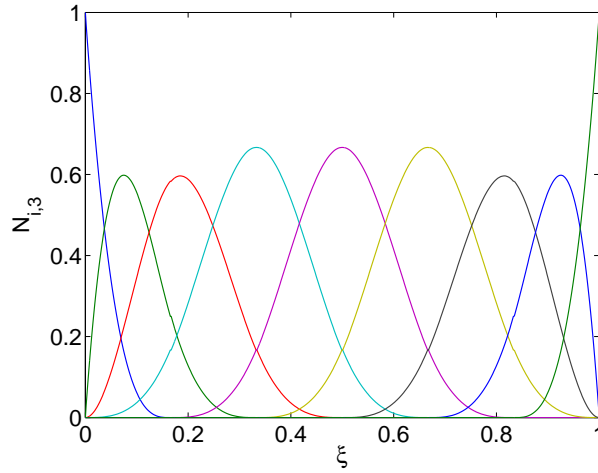


Fig. 1. Cubic basis functions formed from the open knot vector $\{0, 0, 0, 0, 1/6, 1/3, 1/2, 2/3, 5/6, 1, 1, 1, 1\}$.

If internal knots are not repeated, B-spline basis functions are C^{p-1} -continuous. If a knot has multiplicity k , the basis is C^{p-k} -continuous at that knot. In particular, when a knot has multiplicity p , the basis is C^0 and interpolates the control point at that location. We define

$$\mathcal{S} = \text{span}\{N_{i,p}(\xi), i = 1, \dots, n\} \quad (4)$$

By means of tensor products, a multi-dimensional B-spline region can be constructed. We discuss here the case of a two-dimensional region, the higher-dimensional case being analogous. Consider the knot vectors $\{\xi_1 = 0, \dots, \xi_{n+p+1} = 1\}$ and $\{\eta_1 = 0, \dots, \eta_{m+q+1} = 1\}$, and an $n \times m$ net of control points $\mathbf{B}_{i,j}$. One

dimensional basis functions $N_{i,p}$ and $M_{j,q}$ (with $i = 1, \dots, n$ and $j = 1, \dots, m$) of order p and q , respectively, are defined from the knot vectors, and the B-spline region is the image of the map $\mathbf{S} : [0, 1] \times [0, 1] \rightarrow \overline{\Omega}$ given by

$$\mathbf{S}(\xi, \eta) = \sum_{i=1}^n \sum_{j=1}^m N_{i,p}(\xi) M_{j,q}(\eta) \mathbf{B}_{i,j}. \quad (5)$$

The two-dimensional parametric space is the domain $[0, 1] \times [0, 1]$. Observe that the two knot vectors $\{\xi_1 = 0, \dots, \xi_{n+p+1} = 1\}$ and $\{\eta_1 = 0, \dots, \eta_{m+q+1} = 1\}$ generate a mesh of rectangular elements in the parametric space in a natural way. Analogous to (4), we define

$$\mathcal{S} = \text{span}\{N_{i,p}(\xi)M_{j,q}(\eta), i = 1, \dots, n, j = 1, \dots, m\} \quad (6)$$

In general, a rational B-spline in \mathbb{R}^d is the projection onto d -dimensional physical space of a polynomial B-spline defined in $(d+1)$ -dimensional homogeneous coordinate space. For a complete discussion see the book by Farin [23] and references therein. In this way, a great variety of geometrical entities can be constructed and, in particular, all conic sections in physical space can be obtained exactly. The projective transformation of a B-spline curve yields a rational polynomial curve. Note that when we refer to the “degree” or “order” of a NURBS curve, we mean the degree or order, respectively, of the polynomial curve from which the rational curve was generated.

To obtain a NURBS curve in \mathbb{R}^2 , we start from a set $\mathbf{B}_i^\omega \in \mathbb{R}^3$ ($i = 1, \dots, n$) of control points (“projective points”) for a B-spline curve in \mathbb{R}^3 with knot vector Ξ . Then the control points for the NURBS curve are

$$[\mathbf{B}_i]_k = \frac{[\mathbf{B}_i^\omega]_k}{\omega_i}, \quad k = 1, 2 \quad (7)$$

where $[\mathbf{B}_i]_k$ is the k^{th} component of the vector \mathbf{B}_i and $\omega_i = [\mathbf{B}_i^\omega]_3$ is referred to as the i^{th} *weight*. The NURBS basis functions of order p are then defined as

$$R_i^p(\xi) = \frac{N_{i,p}(\xi)\omega_i}{\sum_{i=1}^n N_{i,p}(\xi)\omega_i}. \quad (8)$$

The NURBS curve is defined by

$$\mathbf{C}(\xi) = \sum_{i=1}^n R_i^p(\xi) \mathbf{B}_i. \quad (9)$$

Analogously to B-splines, NURBS basis functions on the two-dimensional

parametric space $\widehat{\Omega} = [0, 1] \times [0, 1]$ are defined as

$$R_{i,j}^{p,q}(\xi, \eta) = \frac{N_{i,p}(\xi)M_{j,q}(\eta)\omega_{i,j}}{\sum_{\hat{i}=1}^n \sum_{\hat{j}=1}^m N_{\hat{i},p}(\xi)M_{\hat{j},q}(\eta)\omega_{\hat{i},\hat{j}}}, \quad (10)$$

where $\omega_{i,j} = (\mathbf{B}_{i,j}^\omega)_3$. Observe that the continuity and support of NURBS basis functions are the same as for B-splines. NURBS spaces are the span of the basis functions (10).

NURBS regions, similarly to B-spline regions, are defined in terms of the basis functions (10). In particular a *single-patch* domain Ω is a NURBS region associated with the $n \times m$ net of control points $\mathbf{B}_{i,j}$, and we introduce the geometrical map $\mathbf{F} : \widehat{\Omega} \rightarrow \overline{\Omega}$ given by

$$\mathbf{F}(\xi, \eta) = \sum_{i=1}^n \sum_{j=1}^m R_{i,j}^{p,q}(\xi, \eta) \mathbf{B}_{i,j}. \quad (11)$$

In order to deal with *multi-patches* geometries, consider N spline and NURBS spaces, defined on $\widehat{\Omega}$, possibly from different knot vectors $\{\xi_{1,k} = 0, \dots, \xi_{n_k+p_k+1,k} = 1\}$ and $\{\eta_{1,k} = 0, \dots, \eta_{m_k+q_k+1,k} = 1\}$ and weights. Denote by $R_{i,j,k}^{p_k,q_k}(\xi, \eta)$ the basis functions on the k -th space and consider then the NURBS maps $\mathbf{F}_k : \widehat{\Omega} \rightarrow \overline{\Omega}_k$

$$\mathbf{F}_k := \sum_{i=1}^{n_k} \sum_{j=1}^{m_k} R_{i,j,k}^{p_k,q_k}(\xi, \eta) \mathbf{B}_{i,j,k}, \quad k = 1, 2, \dots, N,$$

where the $\overline{\Omega}_k \subset \mathbb{R}^2$ represent the *patches* which compose the connected (closed) *physical domain*

$$\overline{\Omega} = \bigcup_{k=1,2,\dots,N} \overline{\Omega}_k.$$

By Ω we indicate the interior part of $\overline{\Omega}$. We assume that the maps $\mathbf{F}_k \in C^1(\widehat{\Omega})$ and their inverses $\mathbf{F}_k^{-1} \in C^1(\Omega_k)$. Moreover we assume that the patches $\overline{\Omega}_k$ form a geometrically conforming multi-patch structure; see for instance figure 3.

Assumption 2.1 (Geometrical conformity) *The common boundary of any two patches is either void, or the image of corners, or the image of edges of $\widehat{\Omega}$. More precisely, we have*

$$\partial\Omega_k \cap \partial\Omega_{k'} = \mathbf{F}_k(E) = \mathbf{F}_{k'}(E') \quad 1 \leq k, k' \leq N,$$

with E, E' either two (possibly coincident) corners or two (possibly coincident) edges of $\widehat{\Omega}$.

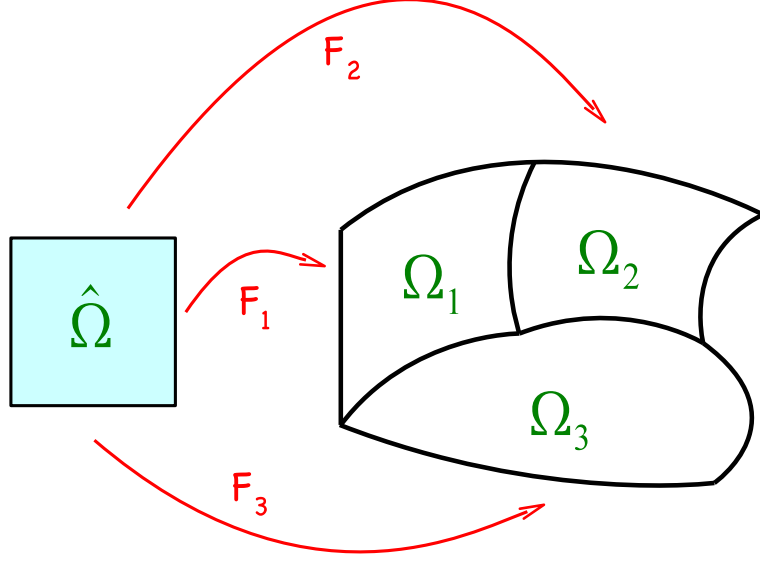


Fig. 2. Example of a domain described by three patches.

Remark 2.1 *The extension to three dimensions is analogous and not discussed.*

2.2 NURBS on the physical domain

Following the isoparametric approach, the space of NURBS vector fields on each patch Ω_k is defined, component by component as the span of the *push-forward* of the basis functions (10)

$$\mathcal{V}_{h,k} = \left[\text{span}\{R_{i,j,k}^{p_k,q_k} \circ \mathbf{F}_k^{-1}, \text{ with } i = 1, \dots, n_k; j = 1, \dots, m_k\} \right]^2. \quad (12)$$

We assume that the spaces $\mathcal{V}_{h,k}$ are conforming at the patch boundaries.

Assumption 2.2 (Space conformity) *With the notation of Assumption 2.1, the spaces $\mathcal{V}_{h,k}|_{\mathbf{F}_k(E)}$ and $\mathcal{V}_{h,k'}|_{\mathbf{F}_{k'}(E')}$ coincide.*

Then, by continuous gluing of (12), we define

$$\mathcal{V}_h = \left\{ \mathbf{v} \in [C^0(\Omega)]^2 : \mathbf{v}|_{\Omega_k} \in \mathcal{V}_{h,k} \right\}. \quad (13)$$

The image of the elements in the parametric space are elements in the physical space. The elements of the physical mesh in Ω_k are therefore

$$\mathcal{T}_k = \left\{ \mathbf{F}_k((\xi_i, \xi_{i+1}) \times (\eta_j, \eta_{j+1})), \text{ with } i = 1, \dots, n_k + p_k, j = 1, \dots, m_k + q_k \right\}. \quad (14)$$

We denote by $\mathcal{T} = \cup_{k=1,2,\dots,N} \mathcal{T}_k$, and by h the mesh-size, that is, the maximum diameter of the elements of \mathcal{T} .

The interested reader may find more details on isogeometric analysis as well as many interesting applications in a number of recently published papers [6,15,16,14,26].

Remark 2.2 *Let E and E' be two edges as in Assumption 2.1. Then, as a consequence of Assumption 2.2, the elements generated on the common boundary $\partial\Omega_k \cap \partial\Omega_{k'}$ by the mappings \mathbf{F}_k and $\mathbf{F}_{k'}$ coincide. The same holds for the two associated knot vectors.*

3 Isogeometric collocation method for elastostatics in a variational context

In this section we follow a variational construction in order to derive the collocation equations. In order to fix ideas, we will concentrate our presentation on the linear elasticity problem.

3.1 Problem description and variational formulation

Let $\Omega \subset \mathbb{R}^d$ represent an elastic body that is subjected to prescribed displacement on part of its boundary Γ_D , and to (possibly null) traction $\mathbf{h} \in [L^\infty(\Gamma_N)]^d$ on the remaining part of the boundary Γ_N . We assume that Γ_D and Γ_N are made of a finite union of connected and regular components. We assume that the traction \mathbf{h} is piecewise continuous, i.e., is continuous on the image of each face (or edge if $d = 2$) of $\widehat{\Omega}$. Regarding the boundary conditions on Γ_D , we make use of a function $\mathbf{g} \in [C^0(\Gamma_D)]^d$ as shown below. The body Ω is also subjected to a volume loading $\mathbf{f} \in [L^\infty(\Omega)]^d$ such that $\mathbf{f}|_{\Omega_k} \in [C^0(\Omega_k)]^d$ for $k = 1, 2, \dots, N$. We indicate with \mathbb{C} the standard fourth-order elasticity tensor. We assume that all components of $\mathbb{C}_k := \mathbb{C}|_{\Omega_k}$ are in $C^1(\Omega_k)$, while we allow \mathbb{C} to have jumps from one patch Ω_k to another. The above regularity requirements on the data can be made weaker; see Remark 3.1 below.

Given the function spaces

$$\begin{aligned} V_{\mathbf{g}} &= \{v \in [H^1(\Omega)]^d : v|_{\Gamma_D} = \mathbf{g}\}, \\ V_0 &= \{v \in [H^1(\Omega)]^d : v|_{\Gamma_D} = 0\}, \end{aligned}$$

the elasticity problem in variational form (based on the principle of virtual work) reads

$$\left\{ \begin{array}{l} \text{Find } \mathbf{u} \in V_{\mathbf{g}} \text{ such that} \\ \int_{\Omega} \mathbb{C} \nabla^S(\mathbf{u}) : \nabla^S(\mathbf{v}) = \int_{\Omega} \mathbf{f} \cdot \mathbf{v} + \int_{\Gamma_N} \mathbf{h} \cdot \mathbf{v} \quad \forall \mathbf{v} \in V_0. \end{array} \right. \quad (15)$$

3.2 A family of discrete problems

In order to simplify the exposition, we extend the function \mathbf{h} by zero on the whole $\cup_{k=1,2,\dots,N} \partial\Omega_k$. Thus \mathbf{h} represents a vector function living on $\cup_{k=1,2,\dots,N} \partial\Omega_k$ whose support is contained in Γ_N . We now assume that the solution \mathbf{u} is in $C^2(\bar{\Omega}_k)$ for all $k = 1, 2, \dots, N$. Then, integrating by parts on each patch Ω_k , $k = 1, 2, \dots, N$, and rearranging terms, equation (15) gives

$$-\sum_{k=1}^N \int_{\Omega_k} \left(\operatorname{div} \mathbb{C}_k \nabla^S(\mathbf{u}) + \mathbf{f} \right) \cdot \mathbf{v} + \sum_{k=1}^N \int_{\partial\Omega_k} \left(\mathbb{C}_k \nabla^S(\mathbf{u}) \cdot \mathbf{n}_k - \mathbf{h} \right) \cdot \mathbf{v} = 0, \quad (16)$$

for all $\mathbf{v} \in V_0$, where \mathbf{n}_k represents the outward unit normal to the domain Ω_k .

We will now consider for simplicity the two-dimensional case $d = 2$, while the extension to three dimensional problems will be discussed afterwards.

We consider the case where the collocation points are chosen using the (tensor-product) *Greville* abscissae [18,20] of the knot vectors. What follows applies also to other sets of collocation points such as, for instance, the *Demko* abscissae, see [20].

Let $k \in \{1, 2, \dots, N\}$. Let $\bar{\xi}_{i,k}$, $i = 1, \dots, n_k$, be the Greville abscissae related to the knot vector $\{\xi_{1,k}, \dots, \xi_{n_k+p_k+1,k}\}$:

$$\bar{\xi}_{i,k} = (\xi_{i+1,k} + \xi_{i+2,k} + \dots + \xi_{i+p_k,k})/p_k. \quad (17)$$

Analogously, let $\bar{\eta}_{j,k}$, $j = 1, \dots, m_k$, be the Greville abscissae related to the knot vector $\{\eta_{1,k}, \dots, \eta_{m_k+q_k+1,k}\}$. It is easy to see that $\bar{\xi}_{1,k} = \bar{\eta}_{1,k} = 0$, $\bar{\xi}_{n_k,k} = \bar{\eta}_{m_k,k} = 1$, while all the remaining points are in $(0, 1)$. We define the collocation points $\hat{\tau}_{i,j,k} \in \hat{\Omega}$ by the tensor product structure

$$\hat{\tau}_{i,j,k} = (\xi_{i,k}, \eta_{j,k}) \in \hat{\Omega},$$

for $i = 1, \dots, n_k$, $j = 1, \dots, m_k$. The collocation points on Ω are then defined accordingly for all $k = 1, 2, \dots, N$ and all i, j as above

$$\tau_{i,j,k} = \mathbf{F}_k(\hat{\tau}_{i,j,k}) \in \Omega_k \subset \Omega.$$

Note that collocation points on $\partial\Omega_k \cap \partial\Omega_{\bar{k}} \neq \emptyset$ coincide because of our conformity assumptions, see Remark 2.2.

Let functions $\delta_{i,j,k}^\varepsilon \in C^\infty(\Omega)$, for $\varepsilon \in \mathbb{R}^+$ and for the same sets of indices i, j, k , as given above, be defined as follows. Let $\varphi : \mathbb{R}^+ \rightarrow \mathbb{R}$ be the C^∞ positive

function

$$\varphi(x) = \begin{cases} e^{1/(x^2-1)} & x \in [0, 1) \\ 0 & x \in [1, +\infty) . \end{cases}$$

We then define the C^∞ radial functions $\psi^\varepsilon : \mathbb{R}^2 \rightarrow \mathbb{R}^+$, depending on the real parameter $0 < \varepsilon \leq 1$, as

$$\psi^\varepsilon(\mathbf{x}) = \varphi(\|\mathbf{x}\|/\varepsilon) \quad \forall \mathbf{x} \in \mathbb{R}^2 ,$$

where $\|\cdot\|$ indicates the euclidean norm. Finally, given any collocation point $\tau_{i,j,k} \in \bar{\Omega}$, for $k = 1, 2, \dots, N$ and $i = 1, \dots, n_k$, $j = 1, \dots, m_k$, we define the functions $\delta_{i,j,k}^\varepsilon$ as

$$\begin{aligned} \delta_{i,j,k}^\varepsilon &: \Omega \longrightarrow \mathbb{R} \\ \delta_{i,j,k}^\varepsilon(\mathbf{x}) &= \psi^\varepsilon(\mathbf{x} - \tau_{i,j,k}) \left(\int_{\Omega} \psi^\varepsilon(\cdot - \tau_{i,j,k}) \right)^{-1} \quad \forall \mathbf{x} \in \bar{\Omega} . \end{aligned} \quad (18)$$

As is evident, $\delta_{i,j,k}^\varepsilon$ is a smoothed Dirac delta function converging to the Dirac delta distribution located at $\tau_{i,j,k}$ as $\varepsilon \rightarrow 0$.

From Lemma A.1 it follows, for all $\mathbf{s} \in [L^\infty(\Omega)]^2$ that are continuous about each $\tau_{i,j,k}$,

$$\lim_{\varepsilon \rightarrow 0} \int_{\Omega} \mathbf{s} \delta_{i,j,k}^\varepsilon = \mathbf{s}(\tau_{i,j,k}), \quad (19)$$

where the integral above is to be calculated component by component.

In order to derive a collocation method from the variational equation (15), we search for a bounded function

$$\mathbf{u}_h \in \mathcal{V}_{h,\mathbf{g}} = \{ \mathbf{v}_h \in \mathcal{V}_h : \mathbf{v}_h(\tau_{i,j,k}) = \mathbf{g}(\tau_{i,j,k}) \quad \forall \tau_{i,j,k} \in \Gamma_D \}$$

that satisfies (16) for all vector test functions $[0, \delta_{i,j,k}^\varepsilon]$ and $[\delta_{i,j,k}^\varepsilon, 0]$, with $k = 1, 2, \dots, N$ and $i = 1, \dots, n_k$, $j = 1, \dots, m_k$. We assume that $\mathcal{V}_h \subset C^0(\Omega) \cap C^2(\cup_k \Omega_k)$, where by $C^2(\cup_k \Omega_k)$ we mean that $\mathbf{u}_h|_{\Omega_k}$ is of class C^2 , for each $k = 1, 2, \dots, N$.

Note that, due to the definition of the discrete space \mathcal{V}_h , we are strongly enforcing the global C^0 continuity of the solution in Ω .

Testing on the above functions gives the following set of equations depending on the parameter ε

$$- \sum_{\bar{k}=1}^N \int_{\Omega_{\bar{k}}} \left(\operatorname{div} \mathbb{C}_{\bar{k}} \nabla^S(\mathbf{u}_h) + \mathbf{f} \right) \delta_{i,j,k}^\varepsilon + \sum_{\bar{k}=1}^N \int_{\partial\Omega_{\bar{k}}} \left(\mathbb{C}_{\bar{k}} \nabla^S(\mathbf{u}_h) \cdot \mathbf{n}_{\bar{k}} - \mathbf{h} \right) \delta_{i,j,k}^\varepsilon = 0 , \quad (20)$$

for $k = 1, 2, \dots, N$, $i = 1, \dots, n_k$, $j = 1, \dots, m_k$, and where as usual an integral of vector functions is calculated component by component.

3.3 Collocation equations

The collocation method is obtained in this section by taking the limit $\varepsilon \rightarrow 0$ of (20). We first consider the simpler case of collocation points that are in the interior of a patch, that is $\tau_{i,j,k} \in \Omega_k$, and then address the more subtle case of collocation points that belong to the patch boundary, that is $\tau_{i,j,k} \in \partial\Omega_k$.

3.3.1 Collocation equations at the patch interior

Let $\tau_{i,j,k} \in \Omega_k$. As noted above, such condition is met if and only if $i \neq 0, j \neq 0$ and $i \neq n_k, j \neq m_k$. In such case, since the support of $\delta_{i,j,k}^\varepsilon$ is contained in the ball of radius ε centered at $\tau_{i,j,k}$, the second term in (20) vanishes for sufficiently small ε . Moreover, for the same range of ε , all the terms but one in the first sum of (20) vanish, thus giving

$$\int_{\Omega_k} \left(\operatorname{div} \mathbb{C}_k \nabla^S(\mathbf{u}_h) + \mathbf{f} \right) \cdot \delta_{i,j,k}^\varepsilon = 0 .$$

Taking the limit for $\varepsilon \rightarrow 0$ in the above equation and recalling (19), we get

$$\left(\operatorname{div} \mathbb{C}_k \nabla^S(\mathbf{u}_h) + \mathbf{f} \right) (\tau_{i,j,k}) = 0, \quad (21)$$

that is, the collocation of the strong form of the equations at $\tau_{i,j,k}$.

3.3.2 Collocation equations at the patch boundary

Assume now $\tau_{i,j,k} \in \partial\Omega_k$. We follow the rules:

- if $\tau_{i,j,k} \in \Gamma_D$ we do not set a collocation equation (however, we have $\mathbf{u}_h(\tau_{i,j,k}) = \mathbf{g}(\tau_{i,j,k})$, since the Dirichlet boundary condition is enforced a priori in $\mathcal{V}_{h,\mathbf{g}}$);
- each $\tau_{i,j,k} \in \Gamma_N$ is associated with a collocation equation, that sets the traction on the boundary Γ_N ;
- the remaining $\tau_{i,j,k} \in \partial\Omega_k$ belong to the inter-patch boundary, and, as already observed; these coincide with other boundary points from other patches; introducing

$$\mathcal{K} = \{ \bar{k} \in \mathbb{N} : 1 \leq \bar{k} \leq N, \tau_{i,j,k} \in \partial\Omega_{\bar{k}} \} . \quad (22)$$

Then $\#\mathcal{K}$, the cardinality of \mathcal{K} , is the number of patches that share $\tau_{i,j,k}$; in this situation we associate to $\tau_{i,j,k}$ a single collocation equation as shown below. Note moreover that, since the space $\mathcal{V}_{h,\mathbf{g}}$ is continuous a priori, there

holds implicitly $\#\mathcal{K} - 1$ gluing conditions, namely

$$\mathbf{u}_h|_{\Omega_{k_1}}(\tau_{i,j,k}) = \mathbf{u}_h|_{\Omega_{k_2}}(\tau_{i,j,k}) = \dots = \mathbf{u}_h|_{\Omega_{k_{\#\mathcal{K}}}}(\tau_{i,j,k}), \quad \text{for } k_1, k_2, \dots, k_{\#\mathcal{K}} \in \mathcal{K}.$$

Considering Section 3.3.1 and the rules above, it is easy to check that the final number of collocation equations corresponds to the size of the discrete space $\mathcal{V}_{h,\mathbf{g}}$.

Considering then $\tau_{i,j,k} \in \partial\Omega_k \setminus \Gamma_D$, we now derive the collocation equation, passing to the limit in (20). Many possibilities arise, some of them are

- I) point $\tau_{i,j,k}$ is on the boundary of a single patch, $\tau_{i,j,k} \in \partial\Omega$ and it is not a corner;
- II) point $\tau_{i,j,k}$ is on the boundary of a single patch and $\tau_{i,j,k}$ is a corner of Ω ;
- III) point $\tau_{i,j,k}$ belongs to the common boundary of two patches Ω_k and is not a corner of both of them (and therefore is inside Ω);
- IV) point $\tau_{i,j,k}$ is a common corner of two or more patches Ω_k ;

and are represented in Figure 3.

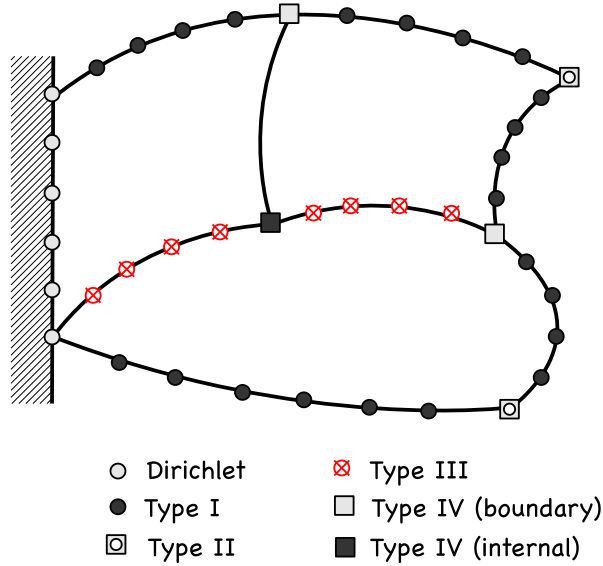


Fig. 3. Example of collocation point types according to Table 1.

The collocation equations in these cases are reported in Table 1, and are derived by the following general approach. Given $\tau_{i,j,k}$, \mathcal{K} as defined in (22) and any $\bar{k} \in \mathcal{K}$, for ε sufficiently small the curve $\partial\Omega_{\bar{k}} \cap \text{supp}(\delta_{i,j,k}^\varepsilon)$ can be divided into two C^0 -connected components $E'_{\bar{k}}$ and $E''_{\bar{k}}$ such that

$$\partial\Omega_{\bar{k}} \cap \text{supp}(\delta_{i,j,k}^\varepsilon) = E'_{\bar{k}} \cup E''_{\bar{k}}, \quad E'_{\bar{k}} \cap E''_{\bar{k}} = \tau_{i,j,k}. \quad (23)$$

Case	Equation
I) $\tau_{i,j,k} \in \partial\Omega$ not a corner point	$(\mathbb{C}_k \nabla^S(\mathbf{u}_h) \cdot \mathbf{n}_k - \mathbf{h})(\tau_{i,j,k}) = 0$
II) $\tau_{i,j,k} \in \partial\Omega$ a corner point, $\mathcal{K} = \{k\}$	$(\mathbb{C}_k \nabla^S(\mathbf{u}_h) \cdot \mathbf{n}'_k - \mathbf{h}')(\tau_{i,j,k}) + (\mathbb{C}_k \nabla^S(\mathbf{u}_h) \cdot \mathbf{n}''_k - \mathbf{h}'')(\tau_{i,j,k}) = 0$
III) $\tau_{i,j,k} \in \partial\Omega_k \cap \partial\Omega_{\bar{k}}$, $\tau_{i,j,k} \notin \partial\Omega$, $\mathcal{K} = \{k, \bar{k}\}$	$(\mathbb{C}_k \nabla^S(\mathbf{u}_h _{\Omega_k}) \cdot \mathbf{n}_k)(\tau_{i,j,k}) + (\mathbb{C}_{\bar{k}} \nabla^S(\mathbf{u}_h _{\Omega_{\bar{k}}}) \cdot \mathbf{n}_{\bar{k}})(\tau_{i,j,k}) \equiv \llbracket \mathbb{C} \nabla^S(\mathbf{u}_h) \cdot \mathbf{n} \rrbracket(\tau_{i,j,k}) = 0$
IV) on the boundary: $\tau_{i,j,k} \in \partial\Omega_k \cap \partial\Omega_{\bar{k}}$, $\tau_{i,j,k} \in \partial\Omega$, $\mathcal{K} = \{k, \bar{k}\}$	$(\mathbb{C}_k \nabla^S(\mathbf{u}_h) \cdot \mathbf{n}'_k - \mathbf{h})(\tau_{i,j,k}) + (\mathbb{C}_{\bar{k}} \nabla^S(\mathbf{u}_h) \cdot \mathbf{n}''_{\bar{k}} - \mathbf{h})(\tau_{i,j,k}) + \llbracket \mathbb{C} \nabla^S(\mathbf{u}_h) \cdot \mathbf{n} \rrbracket(\tau_{i,j,k}) = 0$
IV) internal to the domain: $\tau_{i,j,k} \in \bigcap_{\ell \in \mathcal{K}} \partial\Omega_\ell$ a corner point, $\tau_{i,j,k} \notin \partial\Omega$, $\mathcal{K} = \{k, \bar{k}, \tilde{k}\}$	$\sum_{\ell \in \mathcal{K}} (\mathbb{C}_\ell \nabla^S(\mathbf{u}_h _{\Omega_\ell}) \cdot \mathbf{n}'_\ell)(\tau_{i,j,k}) + (\mathbb{C}_\ell \nabla^S(\mathbf{u}_h _{\Omega_\ell}) \cdot \mathbf{n}''_\ell)(\tau_{i,j,k}) = 0$

Table 1

Some examples of the boundary equations, i.e., assuming $\tau_{i,j,k} \in \partial\Omega_k$ with $\tau_{i,j,k} \notin \Gamma_D$. We refer to Figures 3 and 4 for a graphical representation of the tabulated examples. The symbol $\llbracket \cdot \rrbracket$ stands for the standard jump operator with \mathbf{n} indicating a unit normal to $\partial\Omega_k \cap \partial\Omega_{\bar{k}}$. The first and second cases are examples of Neumann boundary conditions. The third case represents a gluing condition between two patches (here $\tau_{i,j,k}$ is not a corner), while the fourth and fifth are a mix of the above. A description of the different cases is presented in the text.

Note that for simplicity of exposition we have left implicit the dependence of E'_k , E''_k on ε . Multiplying (20) by the positive parameter ε yields, for sufficiently small ε ,

$$-\varepsilon \sum_{\bar{k} \in \mathcal{K}} \int_{\Omega_{\bar{k}}} \left(\operatorname{div} \mathbb{C}_{\bar{k}} \nabla^S(\mathbf{u}_h) + \mathbf{f} \right) \delta_{i,j,k}^\varepsilon + \varepsilon \sum_{\bar{k} \in \mathcal{K}} \int_{\partial\Omega_{\bar{k}}} \left(\mathbb{C}_{\bar{k}} \nabla^S(\mathbf{u}_h) \cdot \mathbf{n}_{\bar{k}} - \mathbf{h} \right) \delta_{i,j,k}^\varepsilon = 0. \quad (24)$$

Due to Lemma A.1 in the appendix, for all $\bar{k} \in \mathcal{K}$ the integral $\int_{\Omega_{\bar{k}}} \left(\operatorname{div} \mathbb{C}_{\bar{k}} \nabla^S(\mathbf{u}_h) + \mathbf{f} \right) \delta_{i,j,k}^\varepsilon$ is bounded independently of ε . Therefore the first term in (24) vanishes in the limit $\varepsilon \rightarrow 0$. Regarding the second term in (24), recalling (23) for all $\bar{k} \in \mathcal{K}$ we can write

$$\begin{aligned} & \varepsilon \int_{\partial\Omega_{\bar{k}}} \left(\mathbb{C}_{\bar{k}} \nabla^S(\mathbf{u}_h) \cdot \mathbf{n}_{\bar{k}} - \mathbf{h} \right) \delta_{i,j,k}^\varepsilon \\ &= \varepsilon \int_{E'_k} \left(\mathbb{C}_{\bar{k}} \nabla^S(\mathbf{u}_h) \cdot \mathbf{n}_{\bar{k}} - \mathbf{h} \right) \delta_{i,j,k}^\varepsilon + \varepsilon \int_{E''_k} \left(\mathbb{C}_{\bar{k}} \nabla^S(\mathbf{u}_h) \cdot \mathbf{n}_{\bar{k}} - \mathbf{h} \right) \delta_{i,j,k}^\varepsilon. \end{aligned} \quad (25)$$

Note that, if $\tau_{i,j,k}$ is a corner point, the two (outward) normal vectors at $\tau_{i,j,k}$ are different for E'_k and E''_k . We therefore indicate with $\mathbf{n}'_{\bar{k}}$ the unit outward (with respect to $\Omega_{\bar{k}}$) normal to E'_k calculated in $\tau_{i,j,k}$. Analogously, we indicate with $\mathbf{n}''_{\bar{k}}$ the unit outward normal to E''_k calculated in $\tau_{i,j,k}$ (see Figure 4). Similarly, since the datum \mathbf{h} is allowed to jump at $\tau_{i,j,k}$, we define \mathbf{h}' and \mathbf{h}'' as the limit values of \mathbf{h} at $\tau_{i,j,k}$ obtained respectively for E'_k and E''_k .

Taking the limit and using Lemma A.2 thus yields

$$\lim_{\varepsilon \rightarrow 0} \varepsilon \int_{E_k^\lambda} \left(\mathbb{C}_{\bar{k}} \nabla^S(\mathbf{u}_h) \cdot \mathbf{n}'_{\bar{k}} - \mathbf{h}' \right) \delta_{i,j,k}^\varepsilon = C_\delta \left(\mathbb{C}_{\bar{k}} \nabla^S(\mathbf{u}_h) \cdot \mathbf{n}'_{\bar{k}} - \mathbf{h}' \right) (\tau_{i,j,k}), \quad (26)$$

and the analogous result holds for E_k'' . Combining all the previous arguments, taking the limit in (24), using (25), (26) and dividing the result by C_δ , finally gives

$$\sum_{\bar{k} \in \mathcal{K}} \left[\left(\mathbb{C}_{\bar{k}} \nabla^S(\mathbf{u}_h) \cdot \mathbf{n}'_{\bar{k}} - \mathbf{h}' \right) (\tau_{i,j,k}) + \left(\mathbb{C}_{\bar{k}} \nabla^S(\mathbf{u}_h) \cdot \mathbf{n}''_{\bar{k}} - \mathbf{h}'' \right) (\tau_{i,j,k}) \right] = 0. \quad (27)$$

Equation (27) enforces the Neumann boundary condition on Γ_N and the normal stress continuity at the inter-patches boundaries.

3.3.3 Final system of equations at the collocation points $\tau_{i,j,k}$

The summary of the equations at the collocation points $\tau_{i,j,k}$ is reported in Table 2.

The final linear system reads as usual

$$\mathbf{K} \bar{\mathbf{u}} = \mathbf{F}, \quad (28)$$

where \mathbf{K} denotes the global stiffness matrix, \mathbf{F} incorporates the body force (\mathbf{f}) and inhomogeneous Dirichlet (\mathbf{g}) and Neumann (\mathbf{h}) boundary conditions (see [25]), and $\bar{\mathbf{u}}$ is the unknown vector of control variables associated to the discrete displacement (\mathbf{u}_h). It is convenient to compute (28) by assembling the contributions from the various patches. Indeed, for all $\tau_{i,j,k} \in \partial\Omega_k$, $k = 1, 2, \dots, N$, equation (28) is nothing but the sum of the contributions from each different patch. This implementation aspect is also discussed in Section 5.3.

Position	Equation
$\tau_{i,j,k} \in \Omega_k$	$(\operatorname{div} \mathbb{C}_k \nabla^S(\mathbf{u}_h) + \mathbf{f})(\tau_{i,j,k}) = 0$
$\tau_{i,j,k} \in \partial\Omega_k$, $\tau_{i,j,k} \notin \Gamma_D$	$\sum_{\bar{k} \in \mathcal{K}} \left[\left(\mathbb{C}_{\bar{k}} \nabla^S(\mathbf{u}_h) \cdot \mathbf{n}'_{\bar{k}} - \mathbf{h}' \right) (\tau_{i,j,k}) + \left(\mathbb{C}_{\bar{k}} \nabla^S(\mathbf{u}_h) \cdot \mathbf{n}''_{\bar{k}} - \mathbf{h}'' \right) (\tau_{i,j,k}) \right] = 0$
$\tau_{i,j,k} \in \Gamma_D$	$\mathbf{u}_h(\tau_{i,j,k}) = \mathbf{g}(\tau_{i,j,k})$, included in the def. of $\mathcal{V}_{h,\mathbf{g}}$

Table 2

Equations at the collocation points $\tau_{i,j,k}$, for $k = 1, 2, \dots, N$ and $i = 1, \dots, n_k$, $j = 1, \dots, m_k$. The set \mathcal{K} is defined in (22). We recall that $\mathbf{h} = \mathbf{0}$ in $\bar{\Omega} \setminus \Gamma_N$, and that for coinciding points ($\tau_{i,j,k} = \tau_{i,j,\bar{k}}$, $k \neq \bar{k}$) the collocation equation is included in the global system only once.

Remark 3.1 *In order to apply the above arguments, we assumed that the data \mathbf{f}, \mathbf{h} are piecewise C^0 and that \mathbb{C} is piecewise C^1 and globally C^0 on Ω .*

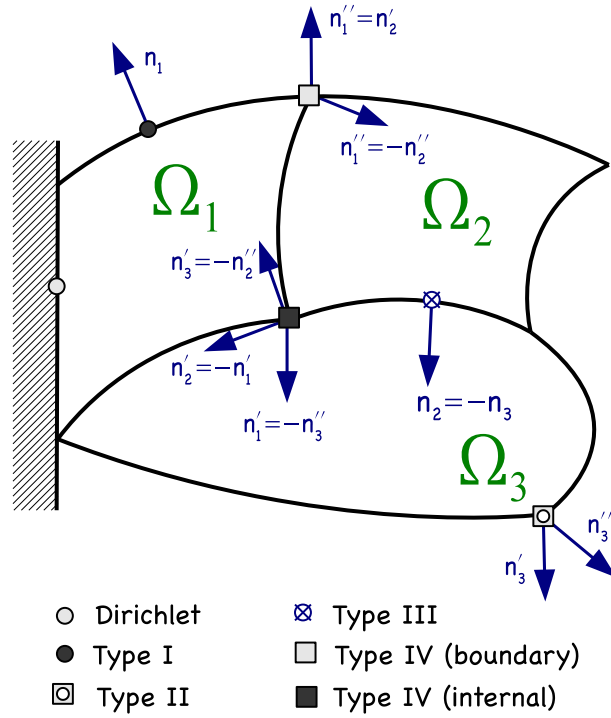


Fig. 4. Example of some collocation points with associated normals.

This continuity conditions on the data \mathbf{h}, \mathbf{f} and on \mathbb{C} are introduced only for simplicity of exposition and can be made weaker. In more general cases, an averaged value of the problem equation at the collocation point needs to be considered.

Remark 3.2 *One can use the same equations listed in Table 2 in the three dimensional case. A variational justification similar to the one we have presented in 2D can be developed also for this case.*

4 Explicit time integration for elastodynamics

In this Section we consider and discuss the extension of our collocation formulation to the elastodynamic case, as well as the explicit predictor multi-corrector algorithm that we employ for time integration.

4.1 Problem description and its algebraic formulation

The elastodynamic problem reads, in variational form,

$$\left\{ \begin{array}{l} \text{Find } \mathbf{u}(t) \in V_{\mathbf{g}} \text{ such that } \forall t \in [0, T] \\ \int_{\Omega} \mathbb{C} \nabla^S(\mathbf{u}(t)) : \nabla^S(\mathbf{v}) + \int_{\Omega} \rho \left(\frac{\partial^2}{\partial t^2} \mathbf{u}(t) \right) \cdot \mathbf{v} = \int_{\Omega} \mathbf{f} \cdot \mathbf{v} + \int_{\Gamma_N} \mathbf{h} \cdot \mathbf{v} \quad \forall \mathbf{v} \in V_0. \end{array} \right. \quad (29)$$

where ρ denotes the material mass density. The equation is the analogue of (15). Discretizing by collocation in space, as detailed in Section 3 for the static problem, we are led to the semidiscrete system of equations

$$\mathbf{K} \bar{\mathbf{u}} + \mathbf{M} \frac{\partial^2}{\partial t^2} \bar{\mathbf{u}} = \mathbf{F}$$

where $\bar{\mathbf{u}} = \bar{\mathbf{u}}(t)$ is the vector of displacement control variables of the discrete (in space) displacement $\mathbf{u}_h(t, \cdot)$, \mathbf{M} denotes the *mass* or *collocation* matrix, \mathbf{K} the stiffness and \mathbf{F} the forcing vector (load plus boundary conditions of Dirichlet and Neumann type) in compact matrix form. Viscous effects may be included as well.

Initial conditions

$$\bar{\mathbf{u}}|_{t=0} = \bar{\mathbf{u}}_0, \quad \frac{\partial}{\partial t} \bar{\mathbf{u}}|_{t=0} = \bar{\mathbf{v}}_0$$

are assigned. See [25] for further details.

4.2 Time integration algorithm

We consider the following explicit predictor multi-corrector time integration algorithm (see [25]): given the acceleration $\bar{\mathbf{a}}_n^{expl} = \bar{\mathbf{a}}_n$, velocity $\bar{\mathbf{v}}_n^{expl} = \bar{\mathbf{v}}_n$ and

displacement $\bar{\mathbf{u}}_n^{expl} = \bar{\mathbf{u}}_n$ at time $t = n\Delta t$, we compute for $r \geq 1$

$$\left\{ \begin{array}{l} \bar{\mathbf{a}}_{n+1}^{(0)} = \mathbf{0}, \\ \bar{\mathbf{v}}_{n+1}^{(0)} = \bar{\mathbf{v}}_n + \Delta t(1 - \gamma)\bar{\mathbf{a}}_n, \\ \bar{\mathbf{u}}_{n+1}^{(0)} = \bar{\mathbf{u}}_n + \Delta t\bar{\mathbf{v}}_n + (1 - 2\beta)\frac{\Delta t^2}{2}\bar{\mathbf{a}}_n, \\ \text{for } i = 0, \dots, r - 1 \\ \quad \mathbf{M}^{expl} \Delta \bar{\mathbf{a}}^{(i)} = \mathbf{F} - \mathbf{M}\bar{\mathbf{a}}_{n+1}^{(i)} - \mathbf{K}\bar{\mathbf{u}}_{n+1}^{(i)}, \\ \\ \quad \bar{\mathbf{a}}_{n+1}^{(i+1)} = \bar{\mathbf{a}}_{n+1}^{(i)} + \Delta \bar{\mathbf{a}}^{(i)}, \\ \quad \bar{\mathbf{v}}_{n+1}^{(i+1)} = \bar{\mathbf{v}}_{n+1}^{(0)} + \gamma \Delta t \bar{\mathbf{a}}_{n+1}^{(i+1)}, \\ \quad \bar{\mathbf{u}}_{n+1}^{(i+1)} = \bar{\mathbf{u}}_{n+1}^{(0)} + \beta \Delta t^2 \bar{\mathbf{a}}_{n+1}^{(i+1)}, \\ \text{end} \end{array} \right. \quad (30)$$

where \mathbf{M}^{expl} denotes the *lumped* mass matrix. Assuming, for the sake of simplicity, a constant density ρ , due to the partition of unity property of NURBS the *lumped* mass matrix becomes $\mathbf{M}^{expl} = \rho \mathbf{I}$, \mathbf{I} being the identity matrix. The load vector \mathbf{F} is evaluated at time $t = (n + 1)\Delta t$. We refer to r as the number of corrector passes. The algorithm produces, after r passes, the following approximations at time $t = (n + 1)\Delta t$

$$\left\{ \begin{array}{l} \bar{\mathbf{a}}_{n+1}^{expl} = \bar{\mathbf{a}}_{n+1}^{(r)}, \\ \bar{\mathbf{v}}_{n+1}^{expl} = \bar{\mathbf{v}}_{n+1}^{(r)}, \\ \bar{\mathbf{u}}_{n+1}^{expl} = \bar{\mathbf{u}}_{n+1}^{(r)}. \end{array} \right. \quad (31)$$

From (30) we derive

$$\begin{aligned} \bar{\mathbf{a}}_{n+1}^{(i+1)} &= \bar{\mathbf{a}}_{n+1}^{(i)} + \Delta \bar{\mathbf{a}}^{(i)} = (\mathbf{I} - (\mathbf{M}^{expl})^{-1}\mathbf{M})\bar{\mathbf{a}}_{n+1}^{(i)} + (\mathbf{M}^{expl})^{-1}(\mathbf{F} - \mathbf{K}\bar{\mathbf{u}}_{n+1}^{(i)}) \\ &= (\mathbf{I} - (\mathbf{M}^{expl})^{-1}(\mathbf{M} + \beta\Delta t^2\mathbf{K}))\bar{\mathbf{a}}_{n+1}^{(i)} + (\mathbf{M}^{expl})^{-1}(\mathbf{F} - \mathbf{K}\bar{\mathbf{u}}_{n+1}^{(0)}). \end{aligned} \quad (32)$$

Iterating, and using $(\mathbf{I} - \mathbf{A})^{-1}\mathbf{v} = \sum_{i=0}^{r-1} \mathbf{A}^i \mathbf{v} + O(\|\mathbf{A}^r \mathbf{v}\|_\infty)$ (where $\|\cdot\|_\infty$ denotes the vector maximum norm), and recalling $\mathbf{M}^{expl} = \rho \mathbf{I}$,

$$\begin{aligned} \bar{\mathbf{a}}_{n+1}^{expl} &= \bar{\mathbf{a}}_{n+1}^{(r)} = \sum_{i=0}^{r-1} (\mathbf{I} - (\mathbf{M}^{expl})^{-1}(\mathbf{M} + \beta\Delta t^2\mathbf{K}))^i (\mathbf{M}^{expl})^{-1}(\mathbf{F} - \mathbf{K}\bar{\mathbf{u}}_{n+1}^{(0)}) \\ &= (\mathbf{M} + \beta\Delta t^2\mathbf{K})^{-1} \mathbf{M}^{expl} (\mathbf{M}^{expl})^{-1}(\mathbf{F} - \mathbf{K}\bar{\mathbf{u}}_{n+1}^{(0)}) \\ &\quad + O(\|(\mathbf{I} - (\mathbf{M}^{expl})^{-1}(\mathbf{M} + \beta\Delta t^2\mathbf{K}))^r (\mathbf{M}^{expl})^{-1}(\mathbf{F} - \mathbf{K}\bar{\mathbf{u}}_{n+1}^{(0)})\|_\infty) \\ &= (\mathbf{M} + \beta\Delta t^2\mathbf{K})^{-1}(\mathbf{F} - \mathbf{K}\bar{\mathbf{u}}_{n+1}^{(0)}) \\ &\quad + O(\|(\mathbf{I} - \rho^{-1}(\mathbf{M} + \beta\Delta t^2\mathbf{K}))^r \rho^{-1}(\mathbf{F} - \mathbf{K}\bar{\mathbf{u}}_{n+1}^{(0)})\|_\infty). \end{aligned} \quad (33)$$

The Newmark algorithm can be written in a similar way: setting $\bar{\mathbf{a}}_n^{Nmk} = \bar{\mathbf{a}}_n$, $\bar{\mathbf{v}}_n^{Nmk} = \bar{\mathbf{v}}_n$ and $\bar{\mathbf{u}}_n^{Nmk} = \bar{\mathbf{u}}_n$, the time step is

$$\left\{ \begin{array}{l} \bar{\mathbf{a}}_{n+1}^{(0)} = 0 \\ \bar{\mathbf{v}}_{n+1}^{(0)} = \bar{\mathbf{v}}_n + \Delta t(1 - \gamma)\bar{\mathbf{a}}_n \\ \bar{\mathbf{u}}_{n+1}^{(0)} = \bar{\mathbf{u}}_n + \Delta t\bar{\mathbf{v}}_n + (1 - 2\beta)\frac{\Delta t^2}{2}\bar{\mathbf{a}}_n \\ (\mathbf{M} + \beta\Delta t^2\mathbf{K})\Delta\bar{\mathbf{a}}^{(0)} = \mathbf{F} - \mathbf{K}\bar{\mathbf{u}}_{n+1}^{(0)} \\ \bar{\mathbf{a}}_{n+1}^{Nmk} = \bar{\mathbf{a}}_{n+1}^{(0)} + \Delta\bar{\mathbf{a}}^{(0)} \\ \bar{\mathbf{v}}_{n+1}^{Nmk} = \bar{\mathbf{v}}_{n+1}^{(0)} + \gamma\Delta t\Delta\bar{\mathbf{a}}_{n+1}^{Nmk} \\ \bar{\mathbf{u}}_{n+1}^{Nmk} = \bar{\mathbf{u}}_{n+1}^{(0)} + \beta\Delta t^2\Delta\bar{\mathbf{a}}_{n+1}^{Nmk}. \end{array} \right. \quad (34)$$

Observe that from (34) we get

$$\bar{\mathbf{a}}_{n+1}^{Nmk} = (\mathbf{M} + \beta\Delta t^2\mathbf{K})^{-1}(\mathbf{F} - \mathbf{K}\bar{\mathbf{u}}_{n+1}^{(0)}). \quad (35)$$

In what follows we present a study whose aim is to obtain some indication of the behavior of the explicit scheme (30).

It is well known that the Newmark algorithm is second-order accurate in time when $\gamma = 1/2$ (see [25]) and as accurate with respect to h as the discretization scheme in space allows. Therefore, for the purpose of investigating the order of the algorithm (30), we compare the solutions of (30)–(31) and (34)–(35) assuming that $\bar{\mathbf{u}}_n^{Nmk} = \bar{\mathbf{u}}_n^{expl} = \bar{\mathbf{u}}_n$, $\bar{\mathbf{v}}_n^{Nmk} = \bar{\mathbf{v}}_n^{expl} = \bar{\mathbf{v}}_n$, $\bar{\mathbf{a}}_n^{Nmk} = \bar{\mathbf{a}}_n^{expl} = \bar{\mathbf{a}}_n$. From (33) and (35) we evaluate a sort of truncation error

$$\begin{aligned} \frac{\|\bar{\mathbf{a}}_{n+1}^{Nmk} - \bar{\mathbf{a}}_{n+1}^{expl}\|_\infty}{\Delta t} &= \frac{1}{\Delta t}O(\|(I - \rho^{-1}(\mathbf{M} + \beta\Delta t^2\mathbf{K}))^r \rho^{-1}(\mathbf{F} - \mathbf{K}\bar{\mathbf{u}}_{n+1}^{(0)})\|_\infty) \\ &= \frac{1}{\Delta t}O(\|\mathbf{B}^r \rho^{-1}(\mathbf{F} - \mathbf{K}\bar{\mathbf{u}}_{n+1}^{(0)})\|_\infty), \end{aligned} \quad (36)$$

where the matrix

$$\mathbf{B} = (I - \rho^{-1}\mathbf{M}) - \rho^{-1}\beta\Delta t^2\mathbf{K} = \rho^{-1}\left((\mathbf{M}^{expl} - \mathbf{M}) - \beta\Delta t^2\mathbf{K} \right). \quad (37)$$

Recalling definitions (30), (31) and (34), we also get

$$\frac{\|\bar{\mathbf{u}}_{n+1}^{Nmk} - \bar{\mathbf{u}}_{n+1}^{expl}\|_\infty}{\Delta t} = \beta\Delta t\|\bar{\mathbf{a}}_{n+1}^{Nmk} - \bar{\mathbf{a}}_{n+1}^{expl}\|_\infty = \Delta tO(\|\mathbf{B}^r \rho^{-1}(\mathbf{F} - \mathbf{K}\bar{\mathbf{u}}_{n+1}^{(0)})\|_\infty), \quad (38)$$

In principle, due to the structure of \mathbf{B} shown in (37), we expect the vector $\mathbf{B}^r\bar{\mathbf{w}}$ to converge to zero for $(h, \Delta t) \rightarrow (0, 0)$, at least when the vector $\bar{\mathbf{w}}$ represents a regular vector field. Moreover, the larger is the exponent r , the higher the

convergence rate expected. Therefore, for sufficiently large values of r , the explicit method is expected to behave like the Newmark method. Numerical tests in the next section will show that *two passes*, i.e., $r = 2$, are in general sufficient to obtain an optimal behavior of the error in h , at least for the cases when $p \leq 5$.

5 Numerical tests: statics

In this section we present the numerical results relative to several 2D plane-strain elasto-static problems, all exploiting the proposed collocation approach, addressing different aspects such as Dirichlet versus Neumann boundary conditions, single-patch versus multi-patch problems, etc. The investigated problems are organized as follows:

- clamped quarter of an annulus, testing a single-patch solution and Dirichlet boundary conditions;
- traction test for a single material, testing a single-patch solution and mixed boundary conditions;
- traction test for a composite material, testing a multi-patch solution and mixed boundary conditions.

In the following we discuss in details each problem.

5.1 *Clamped quarter of an annulus*

We consider a quarter of an annulus, as sketched in Figure 5, with internal and external radii equal to $R_1 = 1$ and $R_2 = 4$, respectively. The domain is exactly represented by a single NURBS patch.

The whole domain boundary is assumed to be clamped and we assign a manufactured solution in terms of displacement components (in the following indicated as *exact*), reading:

$$\begin{cases} u = (x^2 + y^2 - 1)(x^2 + y^2 - 16) \sin(x) \sin(y), \\ v = (x^2 + y^2 - 1)(x^2 + y^2 - 16) \sin(x) \sin(y). \end{cases} \quad (39)$$

The manufactured solution satisfies the prescribed boundary conditions and the load is computed starting from the manufactured solution and imposing equilibrium.

In Figure 6 we present the results in terms of relative solution error in the

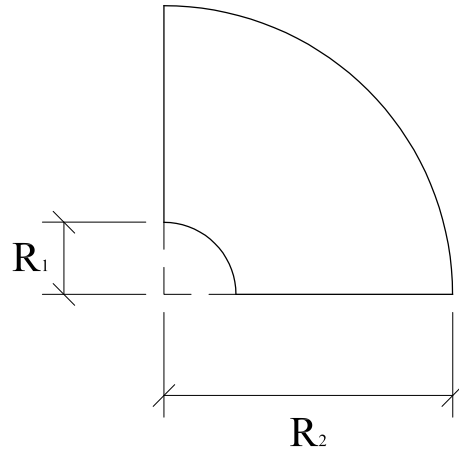


Fig. 5. Clamped quarter of an annulus. Problem geometry.

L^2 -norm versus the square root of the total number of control points used, reporting as a reference the convergence rates discussed in [3], i.e., p and $p - 1$ for even and odd degree p , respectively.

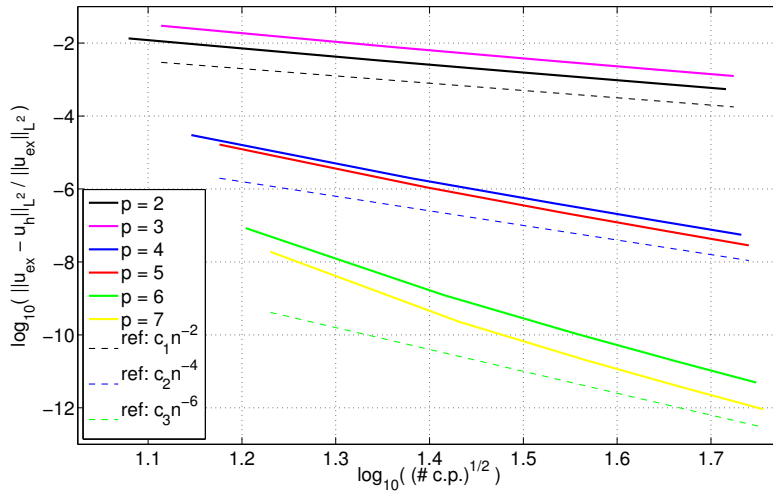


Fig. 6. Clamped quarter of an annulus. Error plot versus the square root of number of control points for different degree NURBS.

5.2 Single-material single-patch traction test

We now consider a square domain Ω of side $L = 1$, subjected to uniform traction, as shown in Figure 7. Accordingly, we specify the following boundary conditions

$$u = 0 \text{ for } x = 0 \text{ and } v = 0 \text{ for } y = 0,$$

while we assume a uniform traction q for $x = L$ and traction-free conditions for $y = L$. The domain consists of a single material and it is represented by a single NURBS patch.

Such a problem allows us to test the proposed numerical scheme for Neumann boundary conditions, described by Equation (27). It is worth emphasizing that it is necessary to explicitly impose not only traction boundary conditions (as in classical Galerkin methods) but also traction-free ones (which are instead naturally satisfied in typical Galerkin methods). Moreover, the problem under investigation is also characterized by a corner (point A in Figure 7) with a combination of traction boundary condition in one direction and traction-free in the other direction, which corresponds to the second case reported in Table 1.

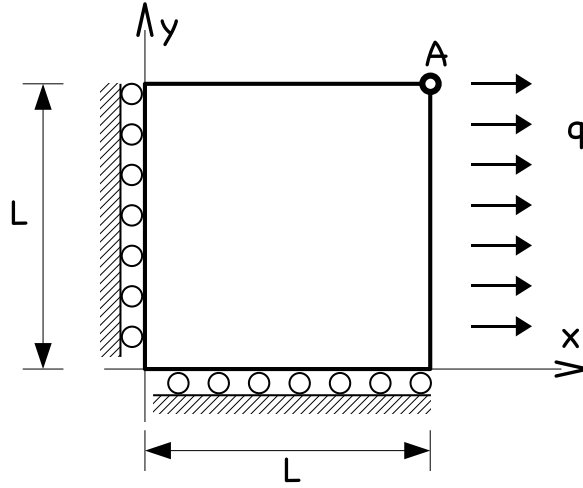


Fig. 7. Single-material single-patch traction test. Problem geometry and boundary conditions.

The analytical problem solution is homogenous and governed by the following set of equations

$$\begin{Bmatrix} \epsilon_{11} \\ \epsilon_{22} \\ \epsilon_{33} \\ \epsilon_{12} \end{Bmatrix} = \frac{1}{E} \begin{bmatrix} 1 & -\nu & -\nu & 0 \\ -\nu & 1 & -\nu & 0 \\ -\nu & -\nu & 1 & 0 \\ 0 & 0 & 0 & 1 - \nu \end{bmatrix} \begin{Bmatrix} \sigma_{11} \\ \sigma_{22} \\ \sigma_{33} \\ \sigma_{12} \end{Bmatrix}. \quad (40)$$

Being in a plane-strain situations, enforcing $\epsilon_{33} = 0$, it is possible to express σ_{33} in terms of σ_{11} and σ_{22} and then, requiring $\sigma_{22} = \sigma_{12} = 0$, it is possible to

compute the solution as

$$\begin{cases} \epsilon_{11} = \frac{1 - \nu^2}{E} \sigma_{11}, \\ \epsilon_{22} = -\frac{\nu}{E} (1 + \nu) \sigma_{11}. \end{cases}$$

Assuming a distributed load per unit length $q = 10$ and material constants $E = 1000$ and $\nu = 0.25$, the displacement components of point A are then

$$u_A = 9.375 \times 10^{-4} \quad , \quad v_A = 3.125 \times 10^{-4}.$$

Such an analytical solution is reproduced up to machine precision by the numerical one computed using a single element, illustrating the good behavior of the proposed numerical scheme for the case under investigation.

Figure 8 shows the horizontal and vertical displacement fields (obtained using $p = q = 2$ and 3×3 control points, i.e., one element), which are linear in the two coordinate variables, as expected.

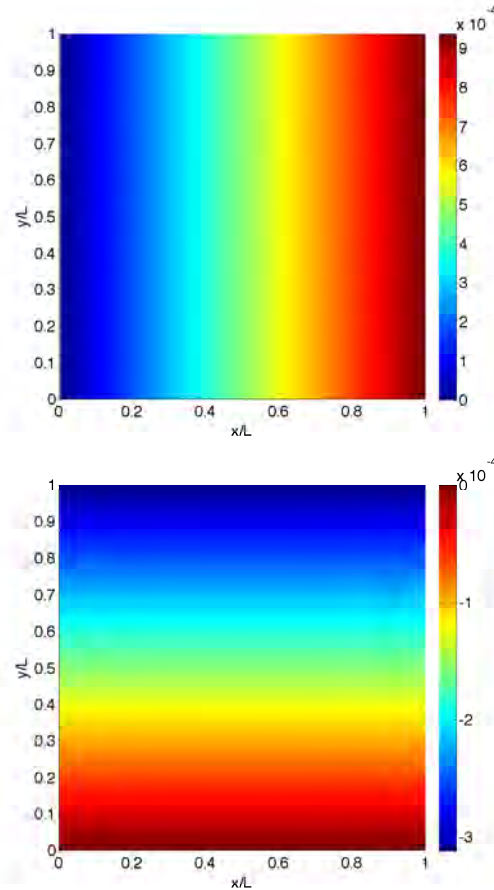


Fig. 8. Single-material single-patch traction test. Horizontal and vertical displacement fields.

5.3 Two-material two-patch traction test

We now consider a rectangular domain Ω , as sketched in Figure 9, again subjected to uniform traction. However, the domain is now assumed to consist of two material subdomains.

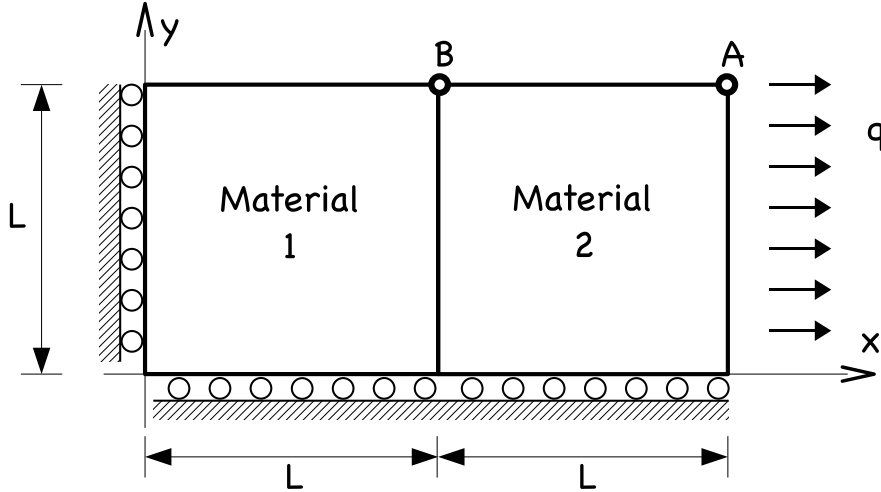


Fig. 9. Two-material two-patch traction test. Problem geometry and boundary conditions.

The problem under investigation is of interest with respect to the previous example, since it introduces a boundary point (point B in Figure 9) with a combination of a traction-free boundary condition and an interface between different materials.

Similarly to what has been done in the previous example, the idea is to reproduce a solution homogeneous in the y direction (and piece-wise homogeneous in the x direction), such that the numerical results should be able to exactly reproduce the analytical solution. However, to obtain such a solution, it is necessary to properly calibrate the elastic constants. Accordingly, recalling that Equations 40 are valid for each material, we require the transverse strain (i.e., the strain in the transverse direction with respect to the traction direction) to be the same in both materials, obtaining the following relation

$$\frac{E_1}{E_2} = \frac{\nu_1(1 + \nu_1)}{\nu_2(1 + \nu_2)},$$

where the subscripts indicate the material numbers.

For the problem under investigation we assume $\nu_1 = 0.2$, $\nu_2 = 0.25$ and $E_2 = 1000$, resulting in $E_1 = 768$. With these material properties, the displacement

of point A (indicated in Figure 9) is then

$$u_A = 2.1875 \times 10^{-3}, \quad v_A = 3.125 \times 10^{-4}.$$

We solve the problem numerically, using two NURBS patches (i.e., a patch for each material). The analytical solution is matched up to machine precision by the numerical one computed using a single element per patch, illustrating the good behavior of the proposed numerical scheme for the case under investigation.

Figure 10 shows the horizontal and vertical displacement fields (obtained using $p = q = 2$ and 3×3 control points per patch, i.e., one element per patch), which are linear in the two coordinate variables within each material, as expected. We also highlight that, as desired, a perfectly homogeneous solution is obtained in the y direction.

We also notice that the management of a conforming multi-patch situation is very simple in the proposed collocation method, since it is based on constructing the discrete equilibrium relation for each patch and, then, summing the equations associated to collocation points shared by multiple patches.

5.4 Pressurized thick-walled cylinder test

We now consider an infinitely long and internally pressurized thick-walled cylinder. We take advantage of the symmetry, considering only a quarter of the cylinder, reducing to the geometry of Figure 5 under plane-strain condition. We impose the following boundary conditions

$$u = 0 \text{ for } x = 0 \text{ and } v = 0 \text{ for } y = 0,$$

and assume a radial pressure load P , uniformly distributed at the inner radius.

For the problem under investigation the exact solution in terms of radial displacement is

$$u_r(r) = \frac{PR_i^2}{E(R_o^2 - R_i^2)} \left[(1 - \nu)r + (1 + \nu)\frac{R_o^2}{r} \right],$$

where r is the radial coordinate, R_i and R_o are the internal and the outer radii, and E and ν are the Young's modulus and Poisson's ratio.

Setting $R_i = 1$ and $R_o = 4$, $E = 1$ and $\nu = 0$, the solution becomes

$$u_r(r) = \frac{P}{15} \left(r + \frac{16}{r} \right).$$

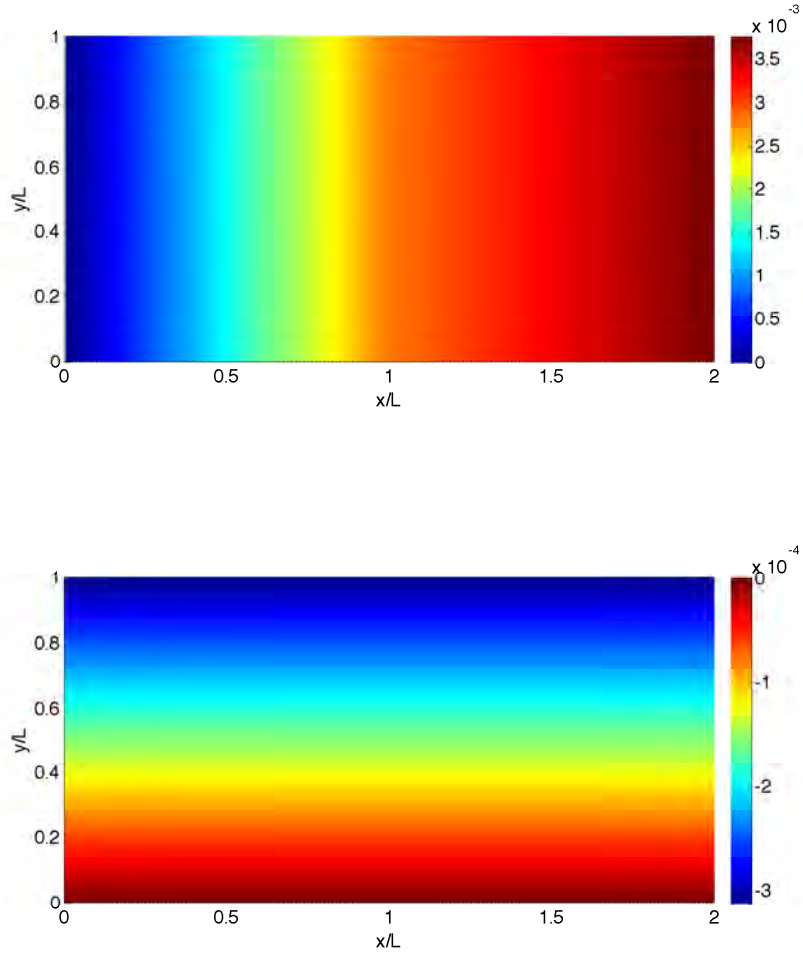


Fig. 10. Two-material two-patch traction test. Horizontal and vertical displacement fields.

Imposing $P = 15/8$, results in

$$u_r(1) = \frac{17}{8} = 2.125 \quad , \quad u_r(4) = 1.$$

In Figure 11 we plot the displacement magnitude obtained using 40×40 control points and $p = q = 4$; note the point-wise (up to machine precision) circumferential symmetry of the solution. In Figure 12 we present the relative solution error in the L^2 -norm versus the square root of the total number of control points.

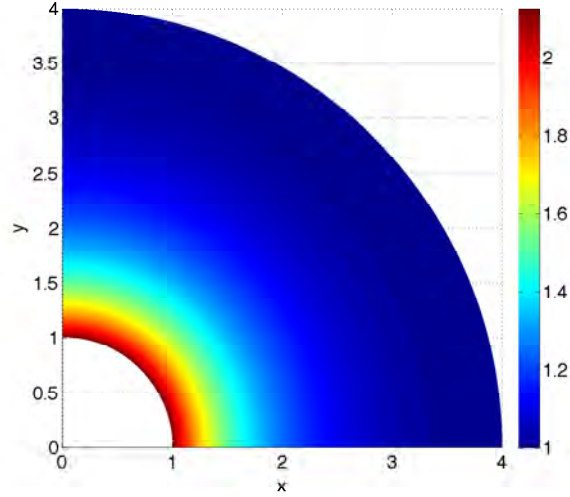


Fig. 11. Pressurized thick-walled cylinder test. Displacement magnitude.

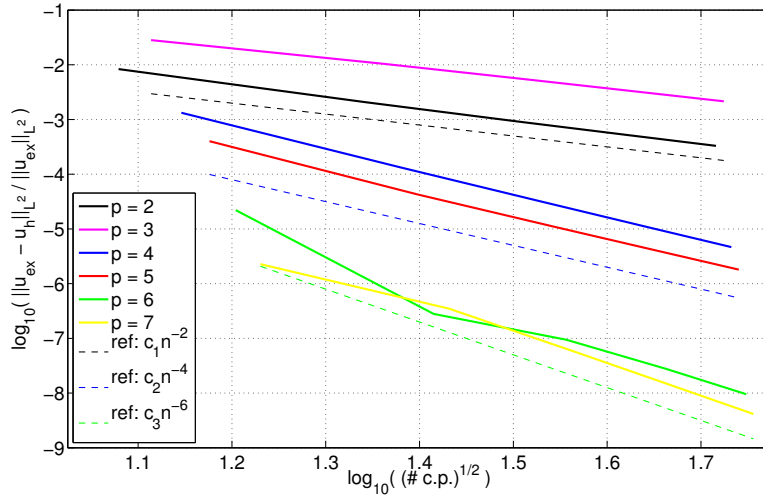


Fig. 12. Pressurized thick-walled cylinder test. Error plot versus the square root of number of control points for different degree NURBS.

6 Numerical tests: dynamics

To solve elastodynamic problems, we employ the explicit predictor multi-corrector algorithm discussed in Section 4. In particular, we present the numerical results of the following two tests:

- a clamped rod, excited by an initial velocity distribution;
- a clamped plane-strain quarter of an annulus, excited by a time-dependent body load and an initial velocity distribution.

6.1 Dynamics of a clamped rod

We consider the 1D elasto-dynamic problem of a rod in a domain $[0, 1]$, governed by the wave equation

$$\ddot{u}(x, t) - u''(x, t) = 0 \quad \forall x \in (0, 1), \forall t \in (0, T), \quad (41)$$

where $u = u(x, t)$ is the unknown displacement in terms of the axial coordinate x and time t , while $(\dot{\cdot})$ and $(\cdot)'$ represent time and space derivatives, respectively.

We consider the following initial conditions

$$u(x, 0) = 0, \quad \dot{u}(x, 0) = 2\pi \sin(2\pi x), \quad \forall x \in (0, 1), \quad (42)$$

and boundary conditions

$$u(0, t) = u(1, t) = 0, \quad \forall t \in (0, T), \quad (43)$$

such that the exact solution is

$$u(x, t) = \sin(2\pi x) \sin(2\pi t). \quad (44)$$

In Figure 13 we present the relative solution error in the L^2 -norm at the final time T ($T = 7/4$ in our simulations), plotted versus the total number of control points. Such numerical solutions are obtained using the explicit predictor multi-corrector algorithm with two corrector passes. We remark that, since the adopted algorithm is only second-order in time, in order to manifest the expected high-order convergence rates in space, the time step and spatial mesh-size must be selected such that the space discretization errors dominate the time discretization errors.

6.2 Dynamics of a clamped plane-strain quarter of an annulus

We consider a 2D plane-strain elastodynamic problem where a clamped quarter of an annulus (whose geometry is described in Figure 5) is excited by a time-dependent body force and an initial velocity distribution such that the exact solution is

$$\begin{cases} u = (x^2 + y^2 - 1)(x^2 + y^2 - 16) \sin(x) \sin(y) \sin(2\pi t), \\ v = (x^2 + y^2 - 1)(x^2 + y^2 - 16) \sin(x) \sin(y) \sin(2\pi t). \end{cases} \quad (45)$$

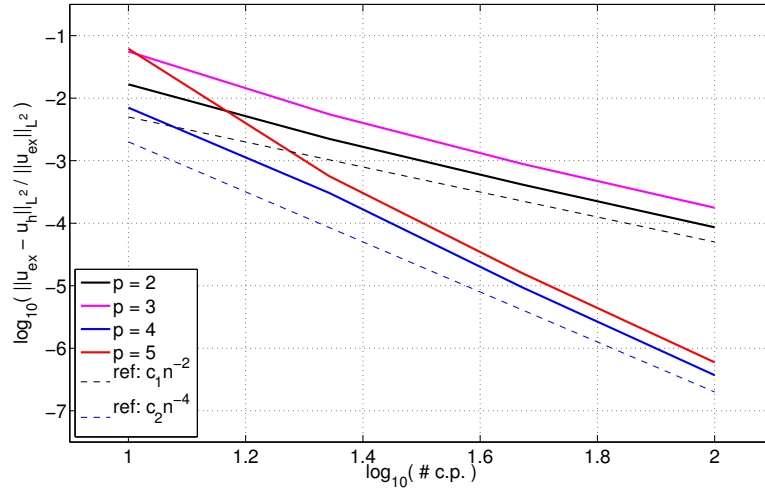


Fig. 13. Dynamics of a clamped rod. Error plot versus number of control points for different degree NURBS.

In Figure 14 we present the relative solution error in the L^2 -norm at the final time T ($T = 7/4$ in our simulations), plotted versus the square root of the total number of control points. Again, such numerical solutions are obtained using the explicit predictor multi-corrector algorithm with two corrector passes. The numerical results are consistent with those obtained in the 1D case. Also here, the time step and spatial mesh-size are selected in order that the space discretization errors dominate the time discretization errors.

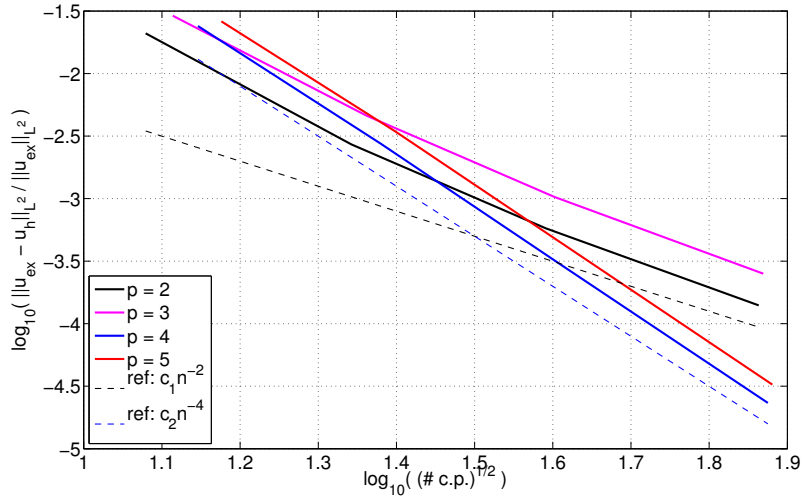


Fig. 14. Dynamics of a clamped plane-strain quarter of an annulus. Error plot versus the square root of number of control points for different degree NURBS.

7 Conclusions

In this paper we have developed IGA collocation formulations applicable to multi-patch NURBS configurations, investigated the treatment of various boundary and patch interface conditions, and extended the methodology to explicit dynamics. We have argued that the procedures are stable, robust, higher-order accurate and efficient in the sense that they involve a minimum number of quadrature points, and we have presented numerical results to support our claims.

We believe that the new methods have the potential to offer a superior alternative to existing finite element technology based on one-point Gaussian quadrature bilinear quadrilateral and trilinear hexahedral elements. However, much research still remains to be done. We believe that the focus of this work should be on fully nonlinear problems, shell formulations, three-dimensional solids, industrial scale calculations, and extension to hierarchically refined NURBS and T-splines, which we hope to pursue in the future.

A Appendix: Construction of $\delta_{i,j,k}^\varepsilon$

We do not show the proof of the following classical result.

Lemma A.1 *Let f, g be real valued functions defined on a neighborhood of $\tau_{i,j,k}$ in Ω . Let f be integrable and continuous in $\tau_{i,j,k}$, and let g be in L^∞ . Then*

$$\begin{aligned} \lim_{\varepsilon \rightarrow 0} \int_{\text{supp}(f)} f \delta_{i,j,k}^\varepsilon &= f(\tau_{i,j,k}) , \\ \int_{\text{supp}(g)} g \delta_{i,j,k}^\varepsilon &\leq C \quad \forall \varepsilon \in (0, 1] , \end{aligned} \tag{A.1}$$

with C a constant independent of ε .

Moreover, the following result is easy to prove.

Lemma A.2 *Let γ be a C^1 curve originating at $\tau_{i,j,k}$. Let f be an integrable real valued function defined on the curve, continuous in $\tau_{i,j,k}$. Then*

$$\varepsilon \lim_{\varepsilon \rightarrow 0} \int_\gamma f \delta_{i,j,k}^\varepsilon = C_\delta f(\tau_{i,j,k}) , \tag{A.2}$$

with C_δ a constant independent of f, ε, γ .

Acknowledgments

F. Auricchio, L. Beirão da Veiga, A. Reali, and G. Sangalli were partially supported by the European Research Council through the FP7 Ideas Starting Grant n. 259229 *ISOBIO* and by the European Commission through the FP7 Factories of the Future project *TERRIFIC*. L. Beirão da Veiga, A. Reali, and G. Sangalli were also partially supported by the European Research Council through the FP7 Ideas Starting Grant n. 205004 *GeoPDEs* and by the Italian MIUR through the FIRB “Futuro in Ricerca” Grant RBFR08CZ0S. T.J.R. Hughes was partially supported by the Office of Naval Research contract number N00014-08-0992, by the Army Research Office contract number W911NF-10-1-0216, and by SINTEF through the ICADA Project. This support is gratefully acknowledged.

References

- [1] I. Akkermann, Y. Bazilevs, V.M. Calo, T.J.R. Hughes, S. Hulshoff. The role of continuity in residual-based variational multiscale modeling of turbulence. *Computational Mechanics*, **41**, 371–378, 2008.
- [2] F. Auricchio, L. Beirão da Veiga, A. Buffa, C. Lovadina, A. Reali, G. Sangalli. A fully “locking-free” isogeometric approach for plane linear elasticity problems: A stream function formulation. *Computer Methods in Applied Mechanics and Engineering*, **197**, 160–172, 2007.
- [3] F. Auricchio, L. Beirão da Veiga, T.J.R. Hughes, A. Reali, G. Sangalli. Isogeometric Collocation Methods. *Mathematical Models and Methods in Applied Sciences*, **20**, 2075–2107, 2010.
- [4] F. Auricchio, L. Beirão da Veiga, C. Lovadina, A. Reali. The importance of the exact satisfaction of the incompressibility constraint in nonlinear elasticity: mixed FEMs versus NURBS-based approximations. *Computer Methods in Applied Mechanics and Engineering*, **199** (5-8): 314–323, 2010.
- [5] F. Auricchio, F. Calabrò, T.J.R. Hughes, A. Reali, G. Sangalli. Efficient Quadrature for NURBS- based Isogeometric Analysis. *ICES-Report 12-04*, 2012.
- [6] Y. Bazilevs, L. Beirão da Veiga, J.A. Cottrell, T.J.R. Hughes, G. Sangalli. Isogeometric analysis: approximation, stability and error estimates for h -refined meshes. *Mathematical Models and Methods in Applied Sciences*, **16**, 1–60, 2006.
- [7] Y. Bazilevs, C. Michler, V.M. Calo, T.J.R. Hughes. Weak Dirichlet boundary conditions for wall-bounded turbulent flows. *Computer Methods in Applied Mechanics and Engineering*, **196**, 4853–4862, 2007.

- [8] Y. Bazilevs, V.M. Calo, J.A. Cottrell, T.J.R. Hughes, A. Reali, G. Scovazzi. Variational Multiscale Residual-based Turbulence Modeling for Large Eddy Simulation of Incompressible Flows. *Computer Methods in Applied Mechanics and Engineering*, **197**, 173–201, 2007.
- [9] L. Beirão da Veiga, A. Buffa, J. Rivas, and G. Sangalli. Some estimates for $h - p - k$ -refinement in isogeometric analysis, *Numer. Math.*, **118**, 271–305, 2011..
- [10] L. Beirão da Veiga, A. Buffa, C. Lovadina, M. Martinelli, G. Sangalli. An isogeometric method for the ReissnerMindlin plate bending problem. *Computer Methods in Applied Mechanics and Engineering*, **209–212**, 45–53, 2012.
- [11] L. Beirão da Veiga, D. Cho and G. Sangalli. Anisotropic NURBS approximation in isogeometric analysis. *Computer Methods in Applied Mechanics and Engineering*, **209-212**: 1–11, 2012.
- [12] D.J. Benson, Y. Bazilevs, M.C. Hsu and T.J.R. Hughes. Isogeometric shell analysis: The Reissner-Mindlin shell. *Computer Methods in Applied Mechanics and Engineering*, **199** (5-8): 276–289, 2010.
- [13] D. J. Benson, Y. Bazilevs, E. De Luycker, M. C. Hsu, M. Scott, T. J. R. Hughes and T. Belytschko. A generalized finite element formulation for arbitrary basis functions: from isogeometric analysis to XFEM. *Inter. J. Numer. Meth. Engrg.*, **83** (6): 765–785, 2010.
- [14] J.A. Cottrell, T.J.R. Hughes, Y. Bazilevs. *Isogeometric Analysis. Towards integration of CAD and FEA*. Wiley, 2009.
- [15] J.A. Cottrell, A. Reali, Y. Bazilevs, T.J.R. Hughes. Isogeometric analysis of structural vibrations. *Computer Methods in Applied Mechanics and Engineering*, **195**, 5257–5296, 2006.
- [16] J.A. Cottrell, T.J.R. Hughes, A. Reali. Studies of Refinement and Continuity in Isogeometric Structural Analysis. *Computer Methods in Applied Mechanics and Engineering*, **196**, 4160–4183, 2007.
- [17] C. de Boor, B. Swartz. Collocation at Gaussian Points. *SIAM Journal on Numerical Analysis*, **10**, 582–606, 1973.
- [18] C. de Boor. *A practical guide to splines*. Springer, 2001.
- [19] C. de Falco, A. Reali, and R. Vázquez, *GeoPDEs: a research tool for isogeometric analysis of PDEs*, *Advances in Engineering Software*, **42**, 1020–1034, 2011.
- [20] S. Demko. On the existence of interpolation projectors onto spline spaces. *Journal of Approximation Theory*, **43**, 151–156, 1985.
- [21] M.R. Dörfel, B. Jüttler, B. Simeon. Adaptive Isogeometric Analysis by Local h -Refinement with T-Splines. *Computer Methods in Applied Mechanics and Engineering*, **199**, 264–275, 2010.

- [22] J.A. Evans, Y. Bazilevs, I. Babuvska and T.J.R. Hughes. n -width, sup-infs, and optimality ratios for the k -version of the isogeometric finite element method. *Computer Methods in Applied Mechanics and Engineering*, **198**: 1726–1741, 2009.
- [23] G.E. Farin. *NURBS curves and surfaces: from projective geometry to practical use*. A.K. Peters, 1995.
- [24] H. Gómez, V. Calo, Y. Bazilevs and T. J. R. Hughes. Isogeometric analysis of the Cahn-Hilliard phase-field model. *Computer Methods in Applied Mechanics and Engineering*, **197**, 4333–4352, 2008.
- [25] T.J.R. Hughes. *The finite element method: Linear static and dynamic finite element analysis*. Dover Publications, 2000.
- [26] T.J.R. Hughes, J.A. Cottrell, Y. Bazilevs. Isogeometric analysis: CAD, finite elements, NURBS, exact geometry, and mesh refinement. *Computer Methods in Applied Mechanics and Engineering*, **194**, 4135–4195, 2005.
- [27] T.J.R. Hughes, K.S. Pister, R.L. Taylor. Implicit-explicit Finite Elements in Nonlinear Transient Analysis. *Computer Methods in Applied Mechanics and Engineering*, **17/18**, 159–182, 1979.
- [28] T.J.R. Hughes, A. Reali, G. Sangalli. Duality and Unified Analysis of Discrete Approximations in Structural Dynamics and Wave Propagation: Comparison of p -method Finite Elements with k -method NURBS. *Computer Methods in Applied Mechanics and Engineering*, **197**, 4104–4124, 2008.
- [29] T.J.R. Hughes, A. Reali, G. Sangalli. Efficient Quadrature for NURBS-based Isogeometric Analysis. *Computer Methods in Applied Mechanics and Engineering*, **199**: 301–313, 2010.
- [30] Y. Kwok, R.D. Moser, J. Jimenez. A Critical Evaluation of the Resolution Properties of B-Spline and Compact Finite Difference Methods. *Journal of Computational Physics*, **174**, 510–551, 2001.
- [31] R.W. Johnson, A B-spline collocation method for solving the incompressible Navier-Stokes equations using an ad hoc method: the Boundary Residual method, *Computers & Fluids*, **34**, (1), 121–149, 2005.
- [32] S. Lipton, J.A. Evans, Y. Basilevs, T. Elguedj, T.J.R. Hughes. Robustness of isogeometric structural discretizations under severe mesh distortions. *Computer Methods in Applied Mechanics and Engineering*, **199**, 357–373, 2010.
- [33] R.Q. Jia. *Spline interpolation at knot averages*, *Constr. Approx.*, **4**, 1–7, 1988.
- [34] L. Piegl and W. Tiller. *The NURBS Book, 2nd Edition*. Springer-Verlag, 1997.
- [35] P.M. Prenter. *Splines and variational methods*. Wiley, 1989.
- [36] A. Reali. An isogeometric analysis approach for the study of structural vibrations. *Journal of Earthquake Engineering*, **10**, s.i. 1, 1–30, 2006.

- [37] D.F. Rogers. *An Introduction to NURBS With Historical Perspective*. Academic Press, 2001.
- [38] L.L. Schumaker. *Spline Functions: Basic Theory*. Krieger, 1993.
- [39] R.L. Taylor. *Isogeometric Analysis of Solids and Structures*. Proceedings of the ECCOMAS Special Interest Conference on Trends and Challenges in Computational Mechanics, Padova, 2011.
- [40] Y. Zhang, Y. Bazilevs, S. Goswami, C.L. Bajaj and T.J.R. Hughes. Patient-specific vascular NURBS modeling for isogeometric analysis of blood flow. *Computer Methods in Applied Mechanics and Engineering*, **196**, 2943–2959, 2007.